Active Tracking Lasers for Precision Target Stabilization

Jim F. Riker
Air Force Research Laboratory Directed Energy Directorate (AFRL/DE)
3550 Aberdeen Ave SE
Kirtland AFB, NM 87117

Abstract

Lasers have historically been considered in the context of weapons, but recent progress has also permitted us to consider using lasers for more subtle applications such as designation, tracking, and discrimination. In this paper, we will review the state of the art of active tracking, including effects such as laser beam quality, diffraction, atmospheric turbulence, and other aspects of laser interactions with the propagation environment. We will present the theory for using lasers in relatively low-power tracking applications.

Keywords: Lasers, illuminators, active tracking, beam control, large optics

Introduction

In this paper, we will review the recent history of active tracking, including modeling for engagements from virtually any platform. We will integrate analysis methodologies developed for several previous active tracking experiments at the AFRL Starfire Optical Range (SOR) to generate predictions for active tracking, using the optical systems at the Maui Space Surveillance System (MSSS) as an example. The techniques for active radiometry have been published previously (ref. 1, 2), but we want to go further here by including the theory for tracking performance itself. Effects such as Noise Equivalent Angle (NEA) errors due to finite SNR, residual atmospheric turbulence-induced tilt, jitter coupling, and speckle are treated. Some of this was previously published as well (ref. 3) so this paper serves mainly as a review to bring it all together and to illustrate some performance results in recent years.

Active tracking requires some new thinking in terms of what we expect to see from the target. For example, when we passively track a solar-lit satellite, we see a reasonably constant signal level as the satellite passes over a short distance in elevation angle. The signal does change slowly, and occasionally we even see short-duration “glints” as the sun temporarily reflects off a natural corner cube composed of satellite edges. With active tracking, these glint effects are expected to be much more frequent, since the beam we are illuminating with is nearly (or perhaps exactly) monostatic with the receiver. Moreover, the atmosphere and other sources of uplink jitter will move the beam rapidly around on the satellite, so that the peak of the beam is only temporarily on any given part of the object. Therefore, the received signal will fluctuate wildly unless we can somehow maintain the tracking and pointing so precisely that this effect is reduced dramatically. That is the crux of active tracking – we must first track the object via some other method as precisely as we can (!) and then

Laser Systems Technology, William E. Thompson, Paul H. Merritt, Editors,
Proceedings of SPIE Vol. 5087 (2003) © 2003 SPIE · 0277-786X/03/$15.00

we must put the beam on the object and attempt to maintain it on the same spot, or at least on some spot.

The interesting features of active tracking are illustrated in figure 1 (ref. 3), where we have both passive and active tracking signals from a particular satellite observed over SOR in March 1997. Looking at the right-hand signals after the break in signal received (near frame 200), the passive signal is reasonably constant at between 500 and 1500 “counts” on a particular camera. The Active Track Laser (ATLAS) is turned on at about frame 300, and the signal then fluctuates wildly from nearly zero to almost 10,000 counts. Note that we generally placed a notch spectral filter in the receiver when we turned the laser on in order to remove as much solar signal as possible, which is why the active signal drops below the passive signal occasionally. Of course, the passive signal does have some significant variation near frame 50, which may have involved low-signal results from the tracker coupled with noise. That variation is seen on occasion.

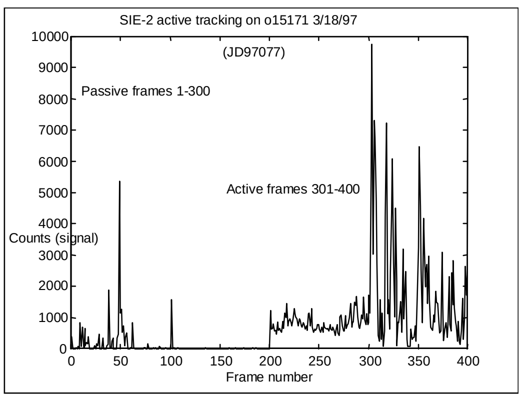

Figure 1. Active and passive returns from an SSN 15171 in March 1997 (ref. 3).

AFRL has also obtained active tracking returns from missile hard-bodies, as illustrated in figures 4 and 5 below (ref. 4, 5). The first graph shows the geometry of the engagement, with the laser engagement occupying the time the missile flies between about 14 degrees elevation and 58 degrees elevation at a horizontal distance near 20 km.

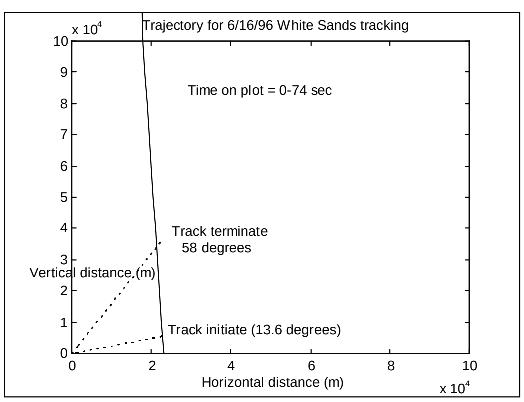

Figure 2. Active tracking engagement geometry for missile tracking (ref. 4, 5).

Figure 3 shows the imagery obtained for this engagement. Going from left to right in the figure, the experimenters first tracked the plume, then turned on the laser to illuminate the hard body, and finally continued tracking actively after the missile burned out. These results were used to help bolster the argument that the Airborne Laser (ABL) could perform its tracking function adequately.

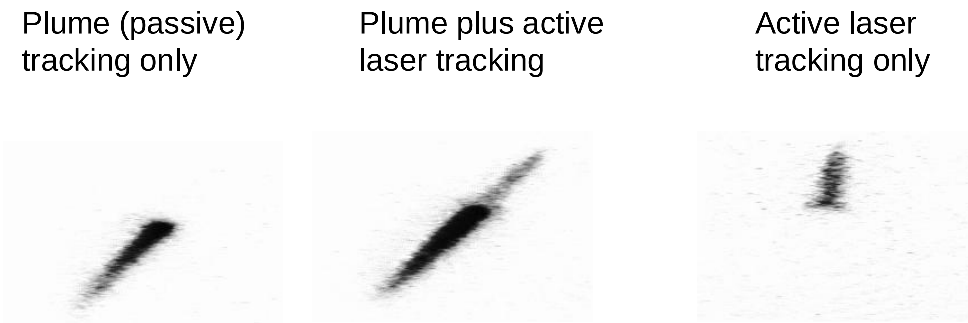

Figure 3. Active tracking imagery from WSMR missile tests (ref. 4, 5).

These early results demonstrated that we could perform active tracking functions, if the lasers were powerful enough (500-w ATLAS) or the missiles close enough. Later, we wished to precisely estimate the radiometry associated with active returns, and we demonstrated that with some high-precision estimates of the satellite Lageos Optical Cross Section (OCS) in August 1997. Figure 4 shows the principal result from that test series (ref. 1), where we compare the measured OCS for the satellite in space against pre-launch NASA laboratory measurements (ref. 6). By precisely measuring the variables associated with the transmitter and receiver, and by precisely measuring atmospheric effects, we were able to obtain 20% RMS agreement in absolute radiometry.

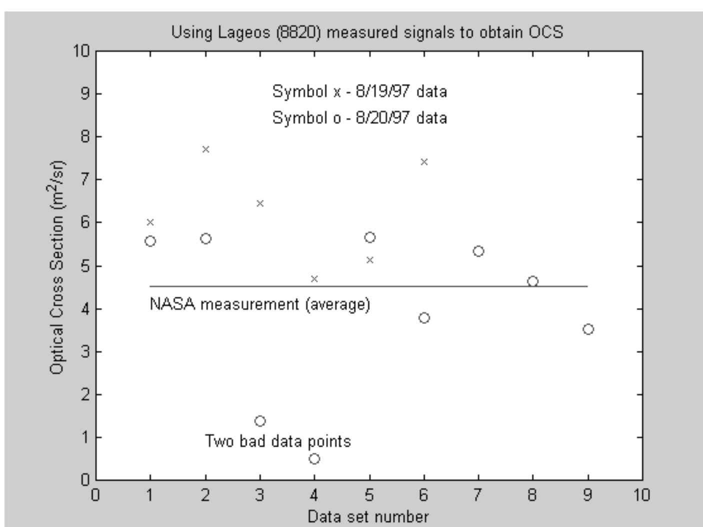

Figure 4. Lageos demonstration of accurate active radiometry (ref. 1).

We should note that each data point plotted was obtained from 30-second laser engagements, where we could be confident that the peak of the laser beam fell on the Lageos satellite. For typical active tracking, we will need some method to estimate the irradiance on the target if we are to replicate this accuracy.

Finally, very recently, we have managed to obtain active returns from unaugmented satellites, as shown in figure 5. We used the Lageos demonstration results and OCS formulas to obtain the active OCS value for these returns, obtaining values in the range 2.3-2.5 m^2/sr (ref. 7).

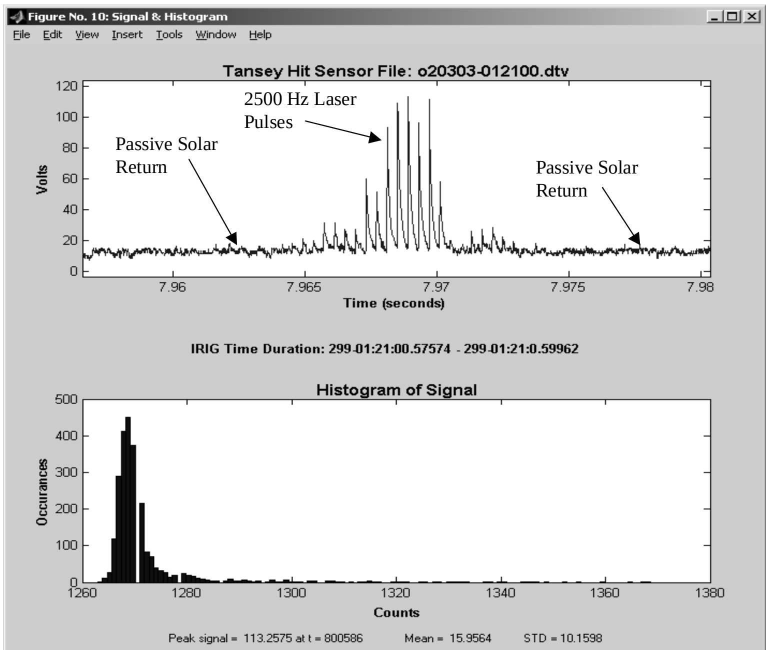

Figure 5. Example of active returns obtained at SOR in August 2002 (ref. 7)

Predictions for tracking performance - general

We can obtain returns from satellites and other tracking targets, so we wish to be able to predict and validate the tracking performance on these objects. To accomplish this, we have developed a number of MATLAB scripts that evaluate the physical effects of radiometry, imperfect illumination of the target, atmospheric turbulence on both the uplink and the downlink paths, and speckle, as they relate to tracking performance. That is, each of these effects contributes as an error source to the perceived motion of the target on a tracking focal plane. Some of them are "real," in the sense of an actual optical motion of the target relative to the tracking observer; examples include radiometry and atmospheric tilt on the downlink path. Others are not, in the sense of being simply a perceived motion of the target even when it has not actually moved –examples include the jitter coupling induced by both the uplink atmospheric tilt and the imperfect illumination of the target. The effects add (in an RMS sense) to produce a total track error. In previous papers, we have published some of these effects, so here we wish to discuss the impact of each of the effects on predicted performance at our AFRL sites.

The most fundamental effect for predicting tracking performance is radiometry. That is, you cannot track what you cannot see. So it is critical to obtain returns from our laser-sensor combination. Of course, the tracking performance is a strong function of the SNR, so we should expect that the more signal we get back, the better we can track. We have published the radiometric formulas in multiple places (ref. 1-4) in different applications, so we are simply reiterating here. For a laser transmitter system, the irradiance profile at a distant target is described as follows (assumes uncompensated turbulence only).

$$
\begin{aligned}
\tilde{w} &= \left[\left(\frac{\beta\lambda z}{\pi w_0}\right)^2 + \left(\frac{\lambda z}{\pi (r_0/2)}\right)^2\right]^{1/2} \\
\tilde{I}_0 &= \frac{2P}{\pi \tilde{w}^2}\tau_{atmosphere,up}^{\sec\psi}\tau_{optics,up} \\
\tilde{I}(\vec{r}) &= \tilde{I}_0 \exp\left(\frac{-2r^2}{\tilde{w}^2}\right)
\end{aligned}
\qquad (1)
$$

The treatment is a gaussian-beam formulation, and we use the waist size w_0 to set the size of the beam exiting the transmitter aperture. The laser wavelength λ, power P and beam quality β, along with the beam waist completely characterize the laser device. The target distance is z, and we assume turbulence is characterized by the Fried coherence diameter r_0. In our formulation, this diameter becomes a limiting aperture in the problem, so that we have to RSS it with the transmitter beam diameter. Of course, there are aperture cutoff effects not explicitly accounted for, so more detailed treatments must include those effects. Also, if we are tracking at the illuminator gimbal, then this formulation does not apply. However, we have developed additional models that treat those effects quite well. This formulation results in a nearly exact illuminator profile at the target, as illustrated in documented previously (ref. 1, 8).

Given the irradiance at the target, we can form the received power, detected electrons, and sensor-reported counts as follows, from standard treatments:

$$
\begin{aligned}
P_{RX} &= \chi I_0 \Omega_{RX}\tau_{atmosphere,down}^{\sec\psi} && \text{(watts) into the aperture} \\
N_e &= P_{RX}\frac{\Delta t\lambda}{hc}\eta(\lambda)\tau_{optical,down}\tau_{spectral} && \text{(electrons) at the detector output} \\
C &= N_e G_{nuc}\kappa && \text{(counts) from the A/D converter}
\end{aligned}
\qquad (2)
$$

There are a number of sensor-related parameters here, but the critical ones are the dwell time Δt, the quantum efficiency η, and the Analog-to-Digital (A/D) conversion factor κ counts/electron. Once we have the total detected signal, we can compute the SNR as shown in equation (3).

The minimum track error due purely to radiometry depends inverse-linearly on the SNR, in a Noise Equivalent Angle (NEA) sense. Tyler and Fried first published results for quad cell type detectors (ref. 9), but the general formula applies, with a different constant of proportionality, to other detectors, equation (4).

$$SNR = \frac{N_e}{\left[N_e + N_{pixels}\sigma^2_{noise}\right]^{1/2}} \qquad \text{radiometric total SNR}$$

$$SNRc = \frac{C}{\left[C + N_{pixels}\sigma^2_{noise-counts}\right]^{1/2}} \qquad \text{total counts or sensor SNR} \tag{3}$$

$$n = \frac{D_{\mathrm{target}} D_{RX}}{\lambda z}$$

$$\sigma_{NEA} = \frac{\pi\lambda\sqrt{\left(\frac{3}{16}\right)^2 + \left(\frac{n}{8}\right)^2}}{D_{RX}\, SNRc} \tag{4}$$

This formulation puts the detector in the "output space" of the receiver telescope in order to find the error due to a quad cell algorithm. Note that in computing the SNR, we should use the average irradiance over the target as opposed to the peak irradiance listed in equations (1) and (2), and we account for that via the following simple formula (ref. 10).

$$\delta = \frac{D_{beam}}{D_{\mathrm{target}}}$$

$$I_{average} = I_0 \frac{\pi\delta^2}{8}\left[erf\left(\frac{\sqrt{2}}{\delta}\right)\right]^2 \tag{5}$$

This average irradiance is used in our model for predicting tracking performance instead of the peak irradiance. We now consider the case of atmospheric turbulence-induced tilts. For the downlink path, the atmosphere introduces a tilt error that represents a true optical motion of the target relative to the receiver. Tyler (ref. 8, 11) has treated this problem in detail, arriving a particular "tracking frequency" or "Tyler frequency" similar to the Greenwood frequency used to characterize higher order adaptive optics. The tracking frequency and associated track error for both raw turbulence (no control loop) and then for a tracking servo loop with closed-loop bandwidth f_{3dB} are given by:

$$f_{\mathrm{T,g-tilt}} = 0.331 D^{-1/6} \lambda^{-1} \sec^{1/2}\psi\left[\int dh C_n^2(h) V^2(h)\right]^{1/2}$$

$$\sigma^2_{\mathrm{atmosphere}}\, 0.170\left(\frac{\lambda}{D}\right)^2\left(\frac{D}{r0}\right)^{5/3} \qquad \text{raw atmosphere} \tag{6}$$

$$\sigma^2_{\mathrm{tracking}} = \left(\frac{f_T}{f_{3dB}}\right)^2\left(\frac{\lambda}{D}\right)^2 \qquad \text{servo residual}$$

For the effect of uplink tilt, we performed a simple analysis using a gaussian beam and a plate target (ref. 12). We analytically jittered the beam on the plate and computed the shift in the centroid that would be perceived. Note what is happening in such a case: the target is not moving at all, but any centroid shifts will be interpreted by a tracker as a target motion. So the tracker will attempt to erroneously follow the perceived track error. The formula for the analytic jitter coupling is as follows:

$$\delta = \frac{D_{\mathrm{beam}}}{D_{\mathrm{target}}}$$

$$J = 1 - \frac{\delta\left[1 - \exp\left(-\frac{8}{\delta^2}\right)\right]}{\sqrt{2\pi}\, erf\left(\frac{2\sqrt{2}}{\delta}\right)} \qquad \text{Jitter coupling fraction} \qquad (7)$$

$$\sigma_{\mathrm{JC}} = \mathrm{J}\alpha_{\mathrm{uplink}} \qquad \text{Jitter coupling tilt RMS}$$

In these equations, the factor α_{uplink} is the RMS uplink tilt error, and the jitter coupling fraction J multiplies that tilt to produce an erroneous perceived tracker tilt. We have compared this analytic treatment of jitter coupling against realistic satellite target 3D models and found excellent agreement in the calculation of the jitter coupling fraction (ref. 13). Figure 6 shows the agreement only between the analytic functions and a MATLAB numerical simulation of the same scenario. However, the data points for the 3D targets essentially bracket the analytic curve.

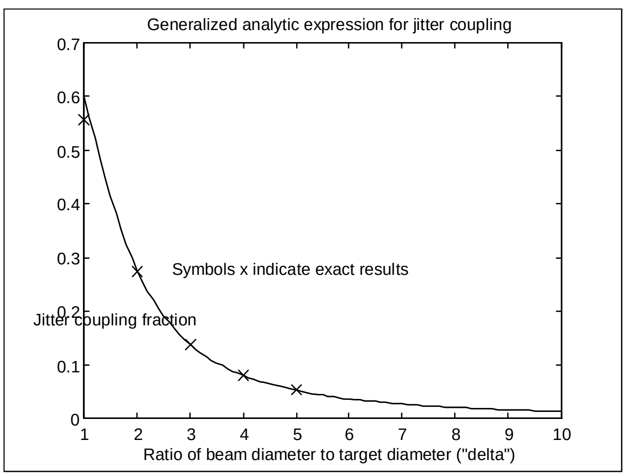

Figure 6. Illustration of jitter coupling fraction agreement for simple plate target.

The final error source we consider in our active tracking model is that of speckle introduced by the interaction of the laser beam with the target micro-structure. Recently, there have been several studies dedicated to analyzing this effect, but we have so far maintained only an older model originally developed by Baribeau (ref. 14). In this model, the track error due to speckle is computed as follows:

$$\sigma^2_{\text{speckle}} = \frac{1}{N_{\text{lasers}}}\left[0.225\frac{\lambda}{D}\right]^2 \tag{8}$$

Strictly speaking, the tracking performance should depend on the power spectrum of the speckle disturbance, but high-fidelity simulations of the effect using TASAT (ref. 15) suggest the spectrum is white over a broad range of temporal frequencies.

Predictions for tracking performance – example for Maui and SOR

The model described above allows us to predict tracking performance for any particular observer tracking any target, though they clearly have some top-level approximations for things like aperture cutoffs, target shape effects, and gaussian beam assumptions. Nevertheless, our model treats very general geometries for observers and targets, allowing us to specify the minimum number of parameters needed to characterize the problem. For the SNR part, we need only the observer altitude, target, and range to the target. More specifically, we can use either the range itself, in which case we can obtain the ground range and zenith angles, or we use the ground range, in which case we compute the range and zenith angles.

Once we have the geometry of the observer and target in an earth-centered frame, we can easily compute by numerical integration the various atmospheric parameters (Fried's coherence diameter r_0, the isoplanatic angle θ_0, the Greenwood frequency f_G, the Tyler or tracking frequency f_T, and the Rytov parameter σ_χ^2. These parameters generally give a top-level description of laser propagation through the atmosphere, and for most tracking problems, r_0 and f_T suffice. For Maui active tracking, we used the parameters in table 1.

Table 1. Parameters used to predict Maui active tracking performance.

Parameter	Symbol	Units	Value
Laser wavelength	λ	μ	1.03
Laser power	P	w	500
Laser beam quality	β	-	1.5
Number of lasers	N_{lasers}	-	16
Transmitter diameter	D_{TX}	m	0.80
Transmitter optical transmission	$\tau_{\text{optical,up}}$	-	0.6
Atmospheric transmission	$\tau_{\text{atmosphere}}$	-	0.7
Atmospheric coherence	r_0	cm	10
Optical Cross Section	χ	m^2/sr	0.1
Receiver diameter	D_{RX}	m	3.6
Receiver optical transmission	$\tau_{\text{optical,down}}$	–	0.30
Detector integration time	Δt	μs	400
Detector Quantum efficiency	η	e/photon	0.60
Detector A/D digitization level	κ	counts/electron	0.1
Detector noise	ν	electrons	80
Tracking control bandwidth	f_{3dB}	Hz	200

These parameters correspond to using the HiBrite 500-w illuminator laser with a precision tracking detector that has not yet been obtained. There are several possibilities for the tracking sensor that are being studied, but we simply wish to estimate performance here. For these parameters, the radiometric performance at various (labeled) target ground ranges and a number of target altitudes is shown in figure 7. We are plotting the sensor-reported SNRc as a function of the engagement zenith angle.

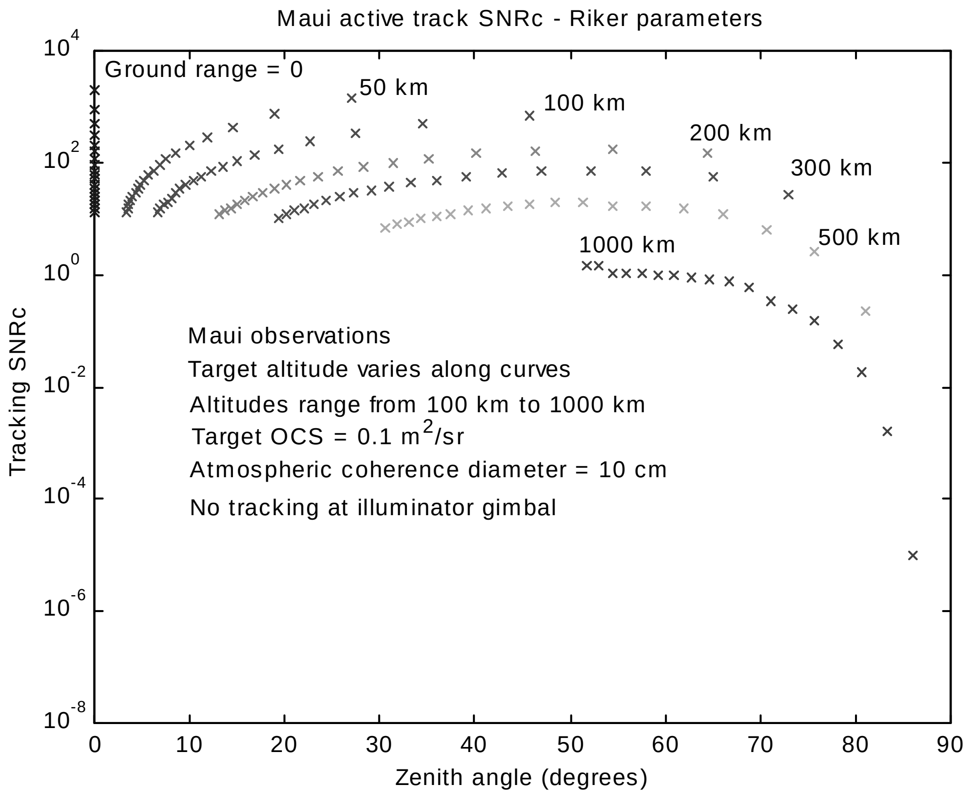

Figure 7. Maui active tracking radiometric performance for a number of engagements.

This particular plot did not assume tracking at the illuminator gimbal, though we will also show results for the case where there is tracking at the illuminator. The combination of target altitudes and ground ranges results in a multitude of cases all plotted on this graph. Each symbol x represents one target-altitude/target-ground-range combination, and the range changes along each set of nearly-connected symbols (i.e., same color symbols). We did use a coherence diameter at 0.5 μ of 10 cm, which is not unusual at the Maui Haleakala site, and found that the tracking SNRc is above 10 for many potential engagements. This is extremely good news, since we used a very low cross section
(0.1 m^2/sr) for our analyses.

Assuming that the radiometry does support closed-loop tracking at Maui on dim and reasonably distant objects, we ran our model to assess the expected tracking performance. In simulations like this, it is possible to distinguish the multiple effects (NEA, residual track error, jitter coupling, speckle) and identify which are the largest error sources. In that way, we can potentially design experiments to single out one or another particular effect. Of course, this is not a trivial matter, as the effects all combine into a single track error presented to the receiver. So we would have to be extremely careful and clever in designing experiments to measure only one effect.

Figure 8 shows our predictions for Maui tracking performance at only two of the many ground ranges shown earlier (viz, 0-km and 1000-km ground range). In this case, we did close the 200-Hz track loops and isolated each particular effect as a function of the transmitter diameter, which has been one critical variable that the Maui design team has assessed. We show the total tilt error as solid blue and green lines for the two ground ranges noted above, and the other major error sources with different line styles.

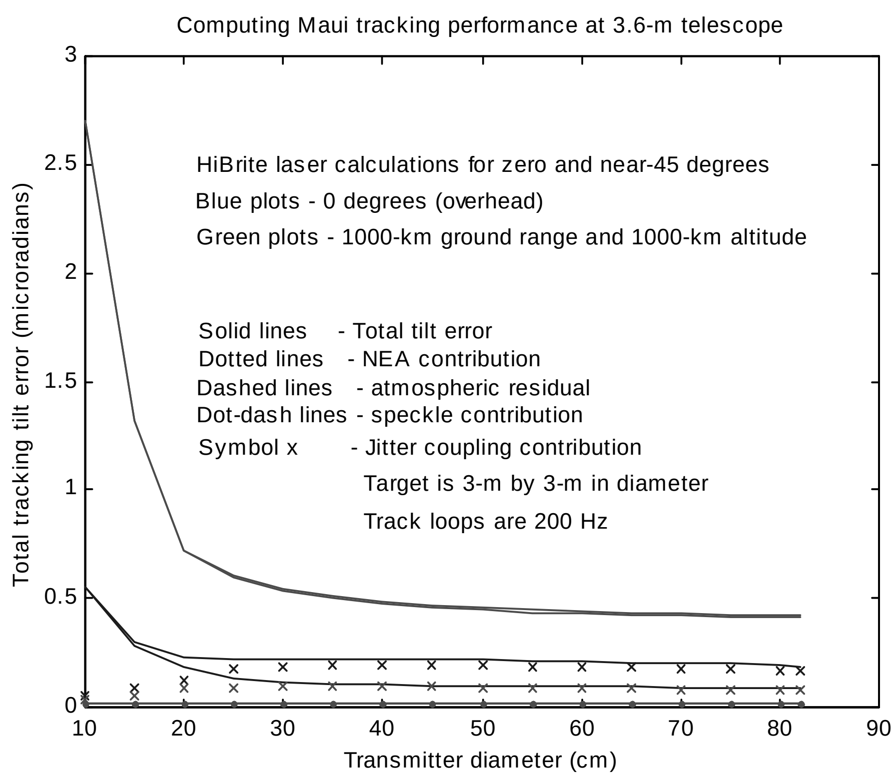

Figure 8. Predicted active tracking error at Maui for parameters in table 1.

Evidently, this plot suggests that the minimum track error occurs at the largest transmitter diameter we can use, with monotonic behavior in track error for smaller transmitters. However, the function is not a strong function for this case, and in fact is essentially flat all the way from small 20-cm transmitters out to the 80-cm transmitter sizes. Why is that? In the case of the off-zenith targets (green plots), the dominant error source is NEA, i.e., pure and simple radiometry. For this case, the track error does decrease noticeably from about 700-nr at 20-cm transmitter sizes to about 450-nr at 80-cm transmitter sizes. So there is a significant tracking benefit to the larger transmitters for the off-zenith cases.

For the overhead cases, the NEA is not the dominant error source; rather, it competes with jitter coupling because of the assumed large size (3-m by 3-m) of the target. Note that at small transmitter sizes, the NEA contribution is large but the jitter coupling contribution is small (because of the large beam at the target). As the transmitter size increases, the NEA gets markedly better, but the decreasing beam size at the target increases the jitter coupling contribution so that the overall performance is relatively flat. This is why analyses like these are important. We can rapidly evaluate the expected performance for different target sizes, ranges, atmospheric conditions, etc. Based on results like this, we would select the large 80-cm transmitter, mainly because of its performance in off-zenith cases where it will be difficult to obtain photons back from the targets. Note that in any real experiment, we are likely to need significant margin to cover unforeseen deleterious effects that make the performance worse than shown here. Thus, since radiometry is fundamental to any tracking performance, we would err on the side of getting photons and worry about any jitter coupling effects later.

Conclusions

In this paper, we have reviewed the theory of active tracking that I have published in various places and applied it to some particular experiments planned for this year at both the AFRL Maui Haleakala test site and the AFRL Starfire Optical Range test site. We have presented a model that captures the predicted performance for very general conditions and obtained results that suggest a few important points:

(1) Active tracking at the two sites is definitely feasible with 500-w class lasers, though the radiometry will not be optimal. This is especially true at Starfire, where the atmospheric seeing is much worse on average than at Maui.
(2) Large transmitters are definitely preferred, simply to maximize the SNR expected in any engagement and hence to minimize the NEA contribution to the track error.
(3) For very large targets in nearly overhead scenarios, jitter coupling does enter the problem and make the benefit of large transmitters less clear. Nevertheless, we obtained the best performance for the largest transmitters even when we included jitter coupling in the cases we ran so far.

We will evaluate the tracking performance experimentally to validate predictions like this in the coming year, attempting to precisely measure the parameters needed to make such predictions. In this way, we expect to reduce risk on any systems that require active tracking in the future.

References

1. Riker, J.F., "Validation of Active Tracking Laser Beam Propagation and Target Signature Predictions," paper 4724-09, SPIE Aerosense Conference, Orlando, Florida, April 2002.
2. Riker, J.F., "Laser requirements for active tracking," Diode Laser Technology Review (DLTR), Albuquerque, NM 6/11/97.
3. Riker, J.F., "Initial results from ATLAS active tracking experiments at SOR," 28th Winter Quantum Electronics Colloquium at Snowbird, January 1998.

4. Riker, J.F., Merritt, P., and J.T. Roark, “Laser requirements for active tracking,” OSA Conference on Non-astronomical adaptive optics,” Munich, Germany, 16 June 1997.
5. Merritt. P.H. and M.A. Kramer, “Active-tracking of Boosting Missiles,” PL-TR-97-1083, May 1997.
6. Fitzmaurice, M.W., Minott, P.O., Abshire, J.B., and H.E. Rowe, “Prelaunch testing of the Laser Geodynamic Satellite (Lageos),” NASA technical paper 1062, October 1977.
7. Kann, J., Crockett, G., and S. Stogsdill, “Optical Cross Section and Active Track Experiment,” technical briefing generated for AFRL, August 2002.
8. Tyler, G.A., “Adaptive Optics: Theory and Applications,” short course and book materials, 12/97.
9. Tyler, G.A. and D.L. Fried, “Image Position Error Associated with a Quadrant Detector,” JOSA v72, #6, pg 804, June 1982.
10. Riker, J.F., “Technical Engineering Memo 97-134: Uplink illuminator beam profiles,” 12/22/97.
11. Tyler, G.A., “Reduction in Antenna Gain due to Random Jitter,” tOSC-TR541, November 1983.
12. Riker, J.F., “TEM 93-20: Analytic treatment of jitter coupling,” 5/21/93.
13. Brunson, R.L., Riker, J.F., and G.A. Crockett, “TEM 97-97: Jitter coupling analysis,” 8/25/97.
14. Baribeau, R., and M. Rioux, “Centroid fluctuations of speckled targets,” Applied Optics, v30, No. 26, 9/10/91.
15. Riker, J.F., Crockett, G.A., and R.L. Brunson, “The time-domain analysis simulation for advanced tracking (TASAT),” SPIE Milestone Series, Selected Papers on Precision Stabilization and Tracking Systems for Acquisition, Pointing, and Control Applications, Volume MS 123, Edited by Michael K. Masten, SPIE Optical Engineering Press, 1996.